Paper 11

Phase field approaches to the kinetic modeling of hydrate phase transitions

Bjørn Kvamme, Atle Svandal, Trygve Buanes, Tatyana Kuznetsova, László Gránásy

Invited and reviewed chapter in a book related to AAPG. Hedberg Research Conference Natural Gas Hydrates: Energy Resource Potential and Associated Geologic Hazards, September 12-16, 2004, Vancouver, BC, Canada, submitted October 2005.

Phase field approaches to the kinetic modeling of hydrate phase transitions.

Bjørn Kvamme[1], Atle Svandal,[1] Trygve Buanes,[1] Tatyana Kuznetsova[1]
[1]*Department of Physics and Technology, University of Bergen, Allégaten 55 , N-5007 Bergen,Norway*

A phase field theory with model parameters evaluated from atomistic simulations/experiments is applied for describing the nucleation and growth and the dissolution of CO_2 hydrate in aqueous solutions under conditions typical to underwater natural gas hydrate reservoirs. It is shown that the size of the critical fluctuations (nuclei) is comparable to the interface thickness, thus the phase field theory predicts a considerably lower nucleation barrier height and higher nucleation rate than the classical approach that relies on a sharp interface. The growth rates of CO_2 hydrate corresponding to different growth geometries (planar, circular, and dendritic) have been determined. The predicted growth rates are consistent with experiments performed under similar conditions. An alternative phase approach based on *cellular automata* has also been formulated and applied to the same model systems. Time dependence for this approach is derived by relating the diffusivity to the interface thickness. For small times the two approaches appear to give similar results but deviates significantly for larger time scales. Dissolution rates of the hydrate phase have been studied as a function of CO_2 concentration in the aqueous solution. On the basis of a simple model of foreign particles, qualitative simulations were performed to describe hydrate formation in porous media. The Avrami-Kolmogorov exponent evaluated from these simulations varies substantially with the volume fraction occupied by the foreign particles.

I. INTRODUCTION

Natural gas hydrates are available in abundance in underwater reservoirs: The amount of carbon bound in natural gas hydrates is conservatively estimated to be twice the amount of carbon to be found in fossil fuels on Earth.[1] Under conditions typical for the underwater hydrate reservoirs (temperatures ranging from –1 °C to a few °C, and pressures in the range of 50 – 100 Bar), the natural gas hydrates can be converted to the significantly more stable CO_2 hydrate in the presence of liquid CO_2 or aqueous CO_2 solution, while natural gas is released. This process is considered as a potential candidate for depositing the ever-increasing quantities of industrial CO_2, as it may become economically beneficial due to the associated natural gas production. Besides offering a way to reduce the emissions to air of one of the most important greenhouse gases, this process might also ease/solve the energy problems expected when exhausting the oil reserves. One of the main obstacles of developing appropriate technologies for the exploitation of the natural gas hydrate reserves is the lack of information on the kinetics of the phase transitions involved. From an environmental point of view the leakage of methane from hydrate reservoirs that are partly exposed at the ocean floor is a growing concern since the effect of methane as a greenhouse gas is of the order of 25 times larger than the corresponding effect of CO_2 per molecule. These exposed hydrate reservoirs are leaking due to a lower chemical potential of methane in the surrounding seawater but the actual leakage rate is a function of the couplings of the hydrate dissociation kinetics to the dynamics of chemical and biological ecosystems that consumes methane as well as the hydrodynamics of the surrounding seawater.

Similar aspects arise when underground hydrate reservoirs are in direct contact with liquid water without any shales or other trapping mechanisms, or when hydrate is in contact with a hydrocarbon phase which is undersaturated with respect to water and hydrate will dissociate in a similar fashion as the sublimation of ice towards air on a cold winter day. Historically these types of hydrate instabilities have caused rapid hydrate dissociations and corresponding catastrophic Tsunamis. The Storegga slide 7000 years ago drowned the lowlands of Scotland[2].

Aquifer storage of CO_2 is already a reality with the injection of Million ton of CO_2 from the Sleipner field into the Utsira formation every year since 1996[3]. The same approach will also be applied for storing the produced CO_2 from fields outside the north of Norway. The low seafloor temperature in these regions may result in regions of CO_2 hydrate formation and a corresponding blocking of the flow. The formation of a hydrate film will, on the hand, at the same time reduce the transport of water and CO_2 across the hydrate film and the film may re-dissociate again if the solution content of CO_2 above the hydrate film falls below the thermodynamic hydrate stability limit.

The dynamic of all these phase transitions are coupled functions of the phase transition kinetics and the related kinetics for transport of heat and mass. A plausible mod-

eling strategy is therefore to apply advanced theoretical concepts in order to evaluate the dominating effects and, on the basis of this, develop simplified kinetic models according to the dominating features of the kinetics as sampled from the more advanced simulations.

In this work we therefore examine two mean field approaches for homogeneous and heterogeneous hydrate growth and hydrate dissociation under different chemical potential gradients between the hydrate and its surroundings. The first approach is the Phase Field Theory (PFT) as applied to hydrate phase transitions[4-13] and the second approach is Cellular Automata (CA)[14] which is also essentially a phase field approach. One of the main differences between the two approaches is that CA uses a Monte Carlo approach to evaluate the progress of the crystal growth, in contrast to PFT which solves a set of coupled differential equations in space and time as derived from a free energy functional for the system.

The paper is structured as follows. In Section II, we describe the phase field model and the cellular automata model used in studying hydrate nucleation and growth, and the molecular dynamics simulations used to investigate the interface properties. In Section III the bulk physical properties of the CO_2 hydrate-aqueous solution system are compiled. In Section IV we present our results: First, the equilibrium properties of the aqueous solution – CO_2 hydrate interface are investigated using molecular dynamics simulations. This is followed by presenting the results of phase field calculations for the formation and dissolution of CO_2 hydrate in aqueous solutions/porous media. Our findings are discussed in Section V, followed by a summary of the results and conclusions in Section VI.

II. Models, thermodynamics and interface properties.

In section IIA we describe the phase field approach while the Cellular Automata approach is described in section IIB. Thermodynamic models for the two approaches are described in section IIC. Molecular dynamics simulations for the interfacial properties are discussed in section IID.

A. Phase field theory

While density functional theory (DFT)[15] utilizes the relationship between the change in structure during a phase transition and the corresponding free energy changes, PFT is based on a free energy functional for the system. For a two-component system undergoing a phase transition from a fluid to a solid, or vice versa, the free energy functional may be written as:

$$F = \int d^3 r \left\{ \tfrac{1}{2}\varepsilon_\phi^2 T(\nabla\phi)^2 + \tfrac{1}{2}\varepsilon_c^2 T(\nabla c)^2 + f(\phi, c) \right\} \quad (1)$$

In these equations the function ϕ, the *phase field*, is a structuring order parameter which monitors the transition between the disordered liquid and ordered crystalline structured. and a conserved field, the coarse-grained CO_2 concentration, c which is equal to the mole fraction divided by the molar volume. Volumetric changes associated with the phase transition is neglected. In equation (1) the phase field is taken to be zero in the solid hydrate phase and unity for the fluid phases. The range of the thermal fluctuations across the interface, associated with a phase transition, is proportional to the width of the interface and the parameters ε_φ and ε_c are proportional to the interface thickness for isotropic growth. f is the free energy of the system per volumetric unit, which may be written as:

$$f(\phi, c) = wTg(\phi) + f_L p(\phi) + f_S \left[(1 - p(\phi)\right] \quad (2)$$

The parameter w is proportional to the interface free energy and the function $g(\phi)$ ensures the double well shape of the free energy functional. The specific form $g(\phi) = {}^1/_4\, \phi^2(1-\phi)^2$ is chosen so as to ensure thermodynamic consistency[12,13] in the PFT formulation. The form of the interpolation function across the phase transition boundary is taken as $p(\phi) = \phi^3(10 - 15\phi + 6\phi^2)$. The resulting differential equations for minimization of free energy, and constrained by conservation of mass is obtained by differentiation of (1):

$$\dot{\phi} = M_\phi \frac{\delta F}{\delta \phi} + \varsigma_\phi \quad (3)$$

$$\dot{c} = \nabla \bullet \left(M_c \nabla \frac{\delta F}{\delta c} \right) + \varsigma_c, \qquad M_c = \frac{D_S + (D_L - D_S)p(\phi)}{RT} \quad (4)$$

where M denote mobilities and D are diffusivity coefficients. Subscripts L and S denote liquid and solid respectively. The applied values are $D_L = 1.0 \cdot 10^{-9}$ m^2/s in the liquid[16] and $D_S = 1.1 \cdot 10^{-12}$ m^2/s for the solid[17] at 1 °C. Same values are adopted for the phase field mobility in equation (3). ζ is an induced noise that mimics the effects of the surroundings beyond the limitations of the simulation box, with subscripts denoting the specific variable. Equations (1) through (4) require no empirical parameters when interface thickness and interface free energy are determined. These properties can be predicted using Molecular Dynamics (MD) simulations. Two approaches have been successfully applied for simple systems like hard spheres and weakly attractive spheres. The first approach estimates the reversible work[18] involved in removing the interface between the two phases while the second approach uses the relationship between interface free energy and the capillary waves at the interface[19-22]. See also section IID. The actual relationships are derived and dis-

cussed in detail elsewhere[23] and only the final equations will be presented here:

$$d = \left(\frac{\varepsilon^2 T}{2} \right)^{1/2} \int_{0.1}^{0.9} d\xi \{ \Delta f[\xi, c(\xi)] \}^{-1/2} \quad (5)$$

where d is the 10 – 90 interface thickness. Manipulations of Eq. (5),[23] gives a corresponding expression for the interface free energy of the solid-liquid interface:

$$\gamma_\infty = (\varepsilon^2 T)^{1/2} \int_0^1 d\xi \{ \Delta f[\xi, c(\xi)] \}^{1/2} \quad (6)$$

where $\Delta f = f - f_0$, and

$$\begin{aligned} f_0 &= f_L(c_L^{eq}) + \left(\frac{\partial f_L}{\partial c}\right)\Big|_{c_L^{eq}} (c - c_L^{eq}) \\ &= f_S(c_S^{eq}) + \left(\frac{\partial f_S}{\partial c}\right)\Big|_{c_S^{eq}} (c - c_S^{eq}) \end{aligned} \quad (7)$$

Equation (7) is the common tangent equation for the equilibrium condition. With appropriate values for d and γ_∞ from experiments or theoretical studies/molecular simulations then equations (5) and (6) can be solved iteratively for ε and w (which comes into Δf through equation (2)).

So far there is not a similar unique approach to predictions of anisotropic growth, which typically requires one or more empirical parameters. An example for a dendritic growth model, which will be applied in our examples, is the following

$$\varepsilon_\phi = \varepsilon_{\phi_0} \left[1 + \frac{s_0}{2} \cos\left(n\vartheta - 2\pi\theta \right) \right] \quad (8)$$

Here s_0 is the anisotropic amplitude, n is the symmetry, θ is the introduced orientation field and $\vartheta = arctan[(\nabla\phi)_y/(\nabla\phi)_x]$. The corresponding differential equation to be integrated along with equations (3) and (4) is:

$$\dot{\theta} = M_\theta \frac{\delta F}{\delta \theta} + \zeta_\theta \quad (9)$$

where $\Im$ is the volumetric free (i.e. the integrand of equation (1)). Extensions to more than two phases and more components are straightforward. Reformation of methane hydrate into CO_2 hydrate can still be modeled with only one phase field describing the transition from fluid phases over to solid hydrate and equation (1) may be extended to:

$$F = \int d\underline{r} \left\{ \begin{array}{l} \frac{\varepsilon_\phi^2 T}{2} (\nabla\phi)^2 + \sum_{i,j=1}^{3} \frac{\varepsilon_{i,j}^2 T}{4} \left(c_i \nabla c_j - c_j \nabla c_i \right)^2 \\ + f_{bulk}(\phi, c_1, c_2, c_3, T) \end{array} \right\} \quad (10)$$

where subscripts i and j denote the three components and the free energy of the bulk is described as:

$$\begin{aligned} f_{bulk} &= wTg(\phi) + [1 - p(\phi)] f_S(c_1, c_2, c_3, T) \\ &+ p(\phi) f_L(c_1, c_2, c_3, T) \end{aligned} \quad (11)$$

For the solid phase free energy in equation (11) the free energy will vary between that of pure methane hydrate towards that of pure CO_2 hydrate as function of the concentrations of water, methane and CO_2 in the hydrate. The fluid region will have a small confined stable region close to the state of pure water, corresponding to the solubility of methane and CO_2 into the aqueous phase. Similarly there will be stable regions close to concentration regions for fluid mixtures of methane and CO_2 and small concentrations of water corresponding to equilibrium solubility of water into these mixtures. This simplified formulation requires a bit caution in defining the mobility of the phase field in equation (3) since it now depends on the source of the components crossing the interface during the phase transition. Extracting CO_2 from supersaturated (with respect to stability with hydrate) aqueous phase into hydrate has a different mobility than extracting the CO_2 from a methane/CO_2 phase. But this can be compensated for by letting the mobility be a function of the concentrations so as to reflect the origin of the phase transition molecules.

$$\dot{\phi} = -M_\phi(c_1, c_2, c_3) \frac{\delta F}{\delta c} + \zeta_\phi \quad (12)$$

The dynamics of the mass transport is similarly extended from equation (4) to yield:

$$\dot{c}_i = \nabla M_{ci}(c_1, c_2, c_3) \nabla \left(\frac{\delta F}{\delta c_i} - \zeta_i \right) \quad (13)$$

with the obvious constraint on conservation of mass

$$\sum_{i=1}^{3} x_i = 1 \quad (14)$$

where x_i are molefractions.

B. Cellular Automata

A cellular automata approach with Monte Carlo samplings of crystal growth[24,25] is briefly outlined below. An extension

The basis of our model is Metropolis tests where the change in free energy as response to change of phase, or change in CO_2 concentration or temperature is considered. As input we use the free energy parameterised with respect to phase, α, where the value 1 corresponds to solid and 0 is fluid. Relative to the continuous PFT description this correspond to the asymptotic values of ϕ =1 for α=0 and ϕ =0 for α=1 for crystal growth from solution. In the following we consider growth of hydrate from solution. x is the mole-fraction of solutes. The total volume is divided into discrete cells. Every change in the system is divided into three steps for every neighbouring cell around the one in consideration. The first step is the solidification, then the mass transport (diffusion) and finally the associated temperature change according to the phase transition enthalpy change. The criteria for solidification are that at least one of the surrounding cells are solid and that:

$$r < \exp\left(-\beta\Delta F_x(x,T)\left[1-\lambda\left\{\Phi-6\right\}\right]\right) \quad (15)$$

where r is a random number between zero and 1 and the subscript x on the free energy indicate the molar free energy as function of the mole-fractions and ΔF_x is the free energy change of the phase transition. β is a characteristic energy. In the second term the constant λ takes into account the effects of the interface and the term Φ is given by:

$$\Phi = \sum_n \omega_n \alpha_n \qquad (16)$$

where the sum over n is over all neighbouring cells and ω_n is a weight for a specific cell. Closest neighbours have weight 2, next-nearest neighbours have weight 1 and more distant cells have zero weight.

The diffusion of CO_2 is done using a Monte Carlo implementation of Fick's law. At each time step one of the nearest neighbours are drawn at random for each cell. The current is given by:

$$j_c = -D_c\Delta\rho_x(1+\delta_c) \quad (17)$$

where ρ_x is proportional to the number density of CO_2 molecules and δ_c is a random number with a Gaussian distribution centred at 0, runs if

$$r < \exp\left[-\beta\Delta f(j_c)\right] \quad (18)$$

where 0 < r < 1 is a random number with a flat distribution, D_c is the diffusivity coefficient, $\Delta f(j_c)$ is the change in free energy due to the current j_c. β is the characteristic energy for the diffusion. In order to keep the volume of each cell constant the CO_2 current is compensated by a water current in the opposite direction.

Due to latent heat the phase transition causes temperature gradients in the system. Temperature diffusion is given by:

$$J_T = -D_T\Delta T(1+\delta_T) \quad (19)$$

where D_T is the thermal diffusion coefficient and δ_T is a random number with a Gaussian distribution centred at 0, is exchanged. In our system the heat transport is much faster than the mass transport. Since equation (19) requires $D_T <$ 1 to be consistent, we must apparently choose D_c very small. But this would slow down the simulation considerably. To circumvent this we replace $D_T \rightarrow D_T$/m and run the temperature diffusion m times. In addition we also need to establish length and time scales since these are not inherently defined in this model. Since the phase can only take the values 0 (liquid) and 1 (solid), but nothing in between, we interpret the size of a cell to be of the same magnitude as the interface thickness between solid hydrate and an aqueous solution. The time scale is connected to the length scale by the diffusion rate.

C. Thermodynamics

The free energy density for the solid hydrate is calculated as

$$\nu_m f_s = \left(\sum_j x_j^{hydrate}\cdot\mu_j^{hydrate}(T,p,\vec{x}^{hydrate})\right) + (1-\sum_j x_j^{hydrate})\mu_w \quad (20)$$

Here $\mu_j^{hydrate}$ and μ_w are the chemical potential of the guest molecule of type *j* and water respectively. In general we have for the molar free energy of the solutes in the liquid phase:

$$G_s = \sum_s x_s\mu^{\infty}{}_s(T,P) + RT\sum_s x_s\ln(x_s\gamma_s) \quad (21)$$

where the infinite symbol indicates infinite dilution as the reference state and subscript s denote solute indices. *R* is the universal gas constant and γ denote activity coefficient of the guest in an aqueous solution in the asymmetric convention (γ_{CO2} is unity in the limit as x goes to zero). For water we have:

$$\mu_w = \mu_w^{pure}(T,P) + RT\ln\left[(1-x)\gamma_w(T,P,\vec{x})\right] \quad (22)$$

Here $\mu^{pure}{}_{w}(T)$ is the chemical potential of pure water,. The activity coefficient of water is obtained through the Gibbs-Duhem relation:

$$\sum_j x_j d\ln(\gamma_j) + \left(1 - \sum_s x_j\right) d\ln(\gamma_w) = 0 \quad (23)$$

The thermodynamic properties can be estimated by considering the equilibrium between liquid and aqueous CO_2/CH_4, $\mu_c^L = \mu_c^{aq}$. Aqueous chemical potentials for solutes are given by the individual terms in Eq. (21) and the fluid thermodynamics can be calculated by a proper equation of state. For the CO_2 system we have used the equation of state by Span and Wagner[26]. Saturation data have been obtained from the model by Diamond and Akinfiev[27]. The chemical potential at infinite dilution is found from molecular dynamics simulations, and for 274.15 K it is $\mu^{\infty}_{CO2} = -19.67$ kJ/mole. This has been taken as a reference level for the absolute thermodynamics, and Eq. (24) has then been applied to obtain the temperature dependence of μ^{∞}_{CO2}.

$$\mu^{\infty}_{CO_2}(T) = \sum_{i=0}^{2} \frac{k_i}{T^i} \qquad (24)$$

The activity coefficient has then been fitted to a polynomial expansion in x.

$$\ln(\gamma_{CO_2}) = \sum_{i=1}^{2} k_i x^i \qquad (25)$$

For the methane a SRK-equation of state[28] has been used, and saturation data have been extracted from the experimental article of Lekvam and Bishnoi[29]. The solubility of methane in water is much less than that of CO_2, for the methane the activity coefficient is assumed to be approximately equal to unity and thus ignored in the calculations. The solubility data have been used to obtain an expression of the chemical potential at infinite dilution.

$$\mu^{\infty}_{CH_4}(T) = \sum_{i=1}^{3} \frac{k_i}{T^i} \qquad (26)$$

All coefficients in Eq. (24-26) are listed in Table 1.

Table 1: Coefficients in Eq. (24-26).

	μ^{∞}_{CO2}	μ^{∞}_{CH4}	$\ln(\gamma_{CO2})$
k_0	$2.94351\cdot10^{4}$	$-6.67663\cdot10^{4}$	0.0
k_1	$-1.58764\cdot10^{7}$	$3.42857\cdot10^{7}$	-1.74497
k_2	$6.61845\cdot10^{8}$	$-5.14493\cdot10^{9}$	$1.06389\cdot10^{2}$

D. Interface properties

The interfacial properties needed to fix ε and w are taken from experiment and atomistic simulations. The experimental value of the free energy of the CO_2 hydrate – aqueous solution interface is $\gamma = 30 \pm 3$ mJ/m^2, evaluated from hydrate dissociation data in mesoporous silica.[30] This magnitude of γ falls close to that of the ice – water interface ($\gamma = 29.1 \pm 0.8$ mJ/m^2)[31].

We used molecular dynamics simulations to evaluate the interfacial density profiles. For this purpose we applied the SPC/E[32] model for water and the model of Harris & Yung[33] for CO_2. The envelope of the interfacial density peaks, which may by loosely identified as the spatial variation of the amplitude of the dominant density wave (i.e., a constant times $\phi(z)$), is fitted with the function

$$X(z) = A + \tfrac{1}{2} B\{1 + \tanh[(z - z_0) / (2^{3/2}\delta)]\}, \quad (27)$$

where the interface thickness δ is related to the 10% – 90% interface thickness d (the distance on which the phase field changes between 0.1 and 0.9) as $d = 2^{5/2}\text{arctanh}(0.8)\,\delta$. Note that this interface profile is strictly valid if the phase field decouples from the concentration field (i.e., chemical effects at the interface are negligible). In practice Eq. (27) seems to approximate the interfacial profiles reasonably well. A snapshot from the simulations plotted in fig. 1. *d* shows some scattering when evaluated from the density or charge density profiles for the two constituents (CO_2 or H_2O). The average value is $d = 0.85 \pm 0.07$ nm. Unless stated otherwise this value has been used to calculate the model parameters of the phase field theory.

A snapshot of an MD simulation is shown in Fig. 1, with the block of hydrate in the center, surrounded by the aqueous phase. Note that the temperature is scaled down in order to reflect that the freezing point of the water model (SPC/E) is significantly lower than the freezing point of real water.

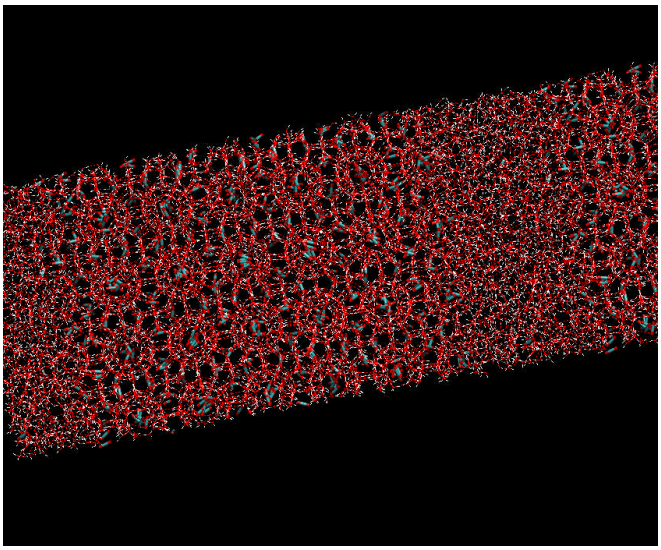

Fig. 1. Snapshot from an MD simulation of CO_2 hydrate in contact with aqueous phase at 200 K and 150 bar.

The respective magnitudes of the free energy parameters are $\varepsilon^2 = 1.23\times10^{-15}$ J/K·cm and $w = 4.82$ J/K·cm^3.

Since water will dominate the interfacial structure and properties we approximately use the same interfacial free energies and interfacial thickness for methane hydrate towards liquid water.

A hypothetical model system: While the calculation of the nucleation barrier and the growth rate are possible with realistic physical properties (though in limited time window for the latter case), a quantitative study of large-scale morphologies or nucleation are practically impossible under such conditions. To gain qualitative knowledge on the general features of the heterogeneous nucleation and growth of CO_2 hydrate in porous media, we introduce a model system that shows qualitative features similar to those of the CO_2 hydrate – aqueous solution system, though providing a considerably larger driving force for hydrate formation. In this hypothetical system, we retain the free energy of the CO_2 hydrate, while replacing the free energy density of the liquid by the following expression:

$$f_L(c) = (1-c)f_1 + cf_2 + f_3(c-c_1)^2(c-c_2)^2, \quad (27)$$

where $f_1 = -2736.19$ J/cm^3, $f_2 = -1437.12$ J/cm^3, $f_3 = 24\,450$ J/cm^3, $c_1 = 0.03$, and $c_1 = 0.97$. The thermodynamic properties of the hypothetical system are compared with those of the real CO_2 hydrate – aqueous solution system in Fig. 2(a).

To reduce further the numerical difficulties in this model system, we assume a broader interface ($d = 3.0$ nm). Then, the relevant values of the free energy parameters read as $\varepsilon^2 = 3.63\times10^{-15}$ J/(K·cm) and $w = 0.0692$ J/(K·cm^3). In the simulations for the model system, the time and spatial steps were chosen as $\Delta t = 0.16\tau$ and $\Delta x = 4\xi$, respectively.

III Hydrate growth simulations

The model has been implemented with both planar and circular geometries for methane and CO_2 hydrate. The temperature is normally chosen to be 1°C to obtain a high driving force without going into the region of ice. Most of the simulations have been done at 150 bars to assure a high driving force. We are assuming no flux boundary conditions at the walls and the grid resolution used is 0.4 nm. The time step is $1.6\cdot10^{-12}$ s. Initially we start with a supersaturated water solution and a hydrate nucleus/film with radius/thickness 4 nm. The supersaturated solution is representing the meta-stable equilibrium between water and liquid CO_2/CH_4. The movement of the front is tracked by following the $\phi=0.5$ value. In Fig. 2 simulations of methane hydrate growth is shown at 3 different pressures.

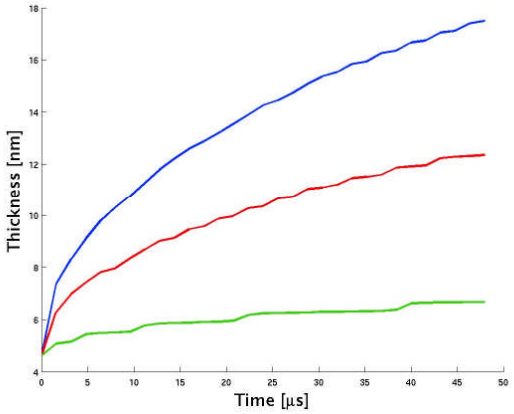

Fig. 2: Thickness of the methane hydrate film as a function of time. Blue line is 150 bars, red line is 100 bars and green line is 50 bars.

For high driving forces (as for CO_2 hydrate and for CH_4 hydrate with circular geometry and high pressure) the simulations follows perfectly a power law $\propto t^{1/2}$ indicating a diffusion controlled process. Under conditions with lower driving forces the simulations shows some deviation from this initially, but the long time behavior converges towards the same power law. Fig. 3 shows the interface velocities for methane and CO_2 hydrate with circular and planar geometries at 1 °C and 150 bars.

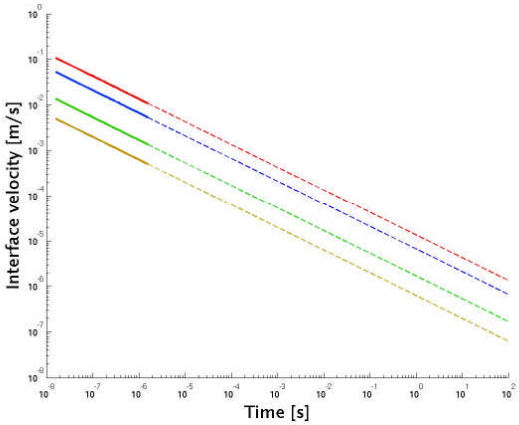

Fig. 3: Velocity of the interface as a function of time. The Solid lines show the actual simulations, while the dashed lines are extrapolations into experimental time-scales. Red line is circular CO_2, blue line is planar CO_2, green line is circular CH_4 and brown line is planar CH_4.

Since the simulations yields the growth process to be determined by the diffusion, three very important parameters in the simulations are the composition in the growing hydrate, the initial mole fraction of the guest molecule in water and the equilibrium mole fraction of the guest molecule between the two phases. Solving simultaneously the equilibrium equations in the two phases with respect to the chemical potential of the components we can obtain the equilibrium conditions at different pressures and tempera-

tures. We find that as we go up in pressure more gas molecules will be available in the solution, and less molecules will be needed to keep the hydrate stable. The fact that the growth rate increases with pressure is better accounted for by this effect than changes in the driving force itself.

In contrast to isotropic growth where the two model parameters ε and w are fixed through information on the interfacial properties there is no similar theoretical relationship to relate anisotropic crystal growth. On the other hand, at the cost of a few empiric model parameters the phase field approach have proven[34,35] to be able to reproduce the growth of many experimentally observed crystal structures. The relative impact of these oriental effects on kinetic growth rates and kinetic limiting contributions is an important issue. For this purpose Eq. (8) applies for ε.

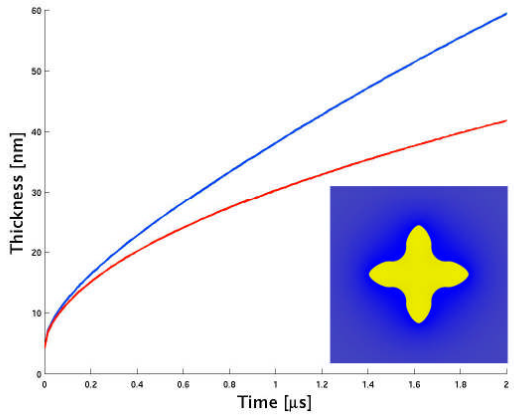

Fig. 4: Anisotropic growth (upper line) compared to isotropic growth (lower line). The picture shows the dendrite the end of the simulated time

In real systems orientation dependencies will evolve naturally since different initial nuclei will have different free energies de-pending on time after nucleation and progress of the growth. This will induce gradients in free energies and as a result smaller and less stable cores may dissociate at the cost of further growth of cores with lower free energy, and corresponding directional gradients in free energy. This is illustrated in fig. 6 where a slab of pure CO_2 is in contact with saturated CO_2 solution. A number of initial hydrate cores are put on the interface as illustrated in 6 (a). Fig.s 6 (b) and (c) shows the non-isotropic growth pattern at the interface at two different times after the initial state.

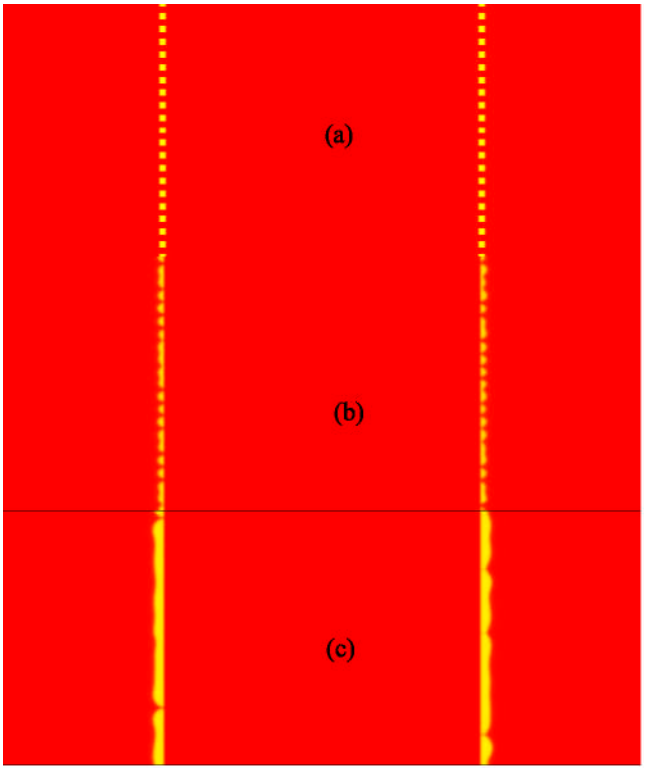

Fig. 6. Hydrate (yellow) growing at the interface between fluid CO_2 phase (inner red region) and saturated CO_2 solution in water (outer red regions) at 150 bar and 1 C and at two different times after initial state in (a). time step in these simulations are 10^{-14} s.

A simple porous system is generated by randomly filling in spherical regions in which there is no flux. In the example below these spheres are taken to be of equal size but there is no limitation in this respect and any type of size and geometries can be constructed. In fig. 7 we illustrate the hydrate growing from saturated solution of CO_2 at 150 bar and 1 C. In particular we note that initiation of growth is favored in in-clines between the particles due to favorable gradients in free energies. It is also possible to extend this type of approach to particles with more realistic interface properties. This can be accomplished using simulated interfacial free energies. Work along this direction is already in progress[32,33,]

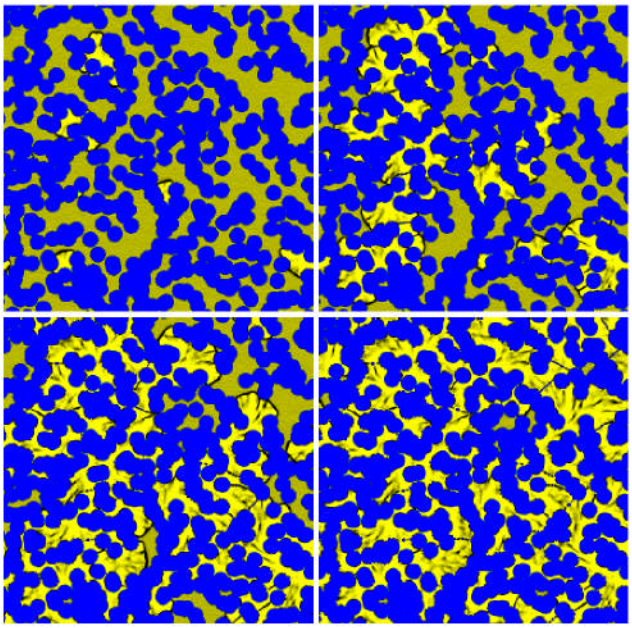

Fig. 7. Simulated hydrate growth in micropores. Blue colour denotes solid material and yellow is hydrate. Time is from left to right and downwards.

The advantage of the cellular automata approach is the numerical efficiency. It is at least one order of magnitude faster. In fig. 7 we compare the results for a growing film of CO_2 hydrate from the two concepts. Results are in fair agreement within the limited time scale of these simulations but the asymptotic behavior deviates

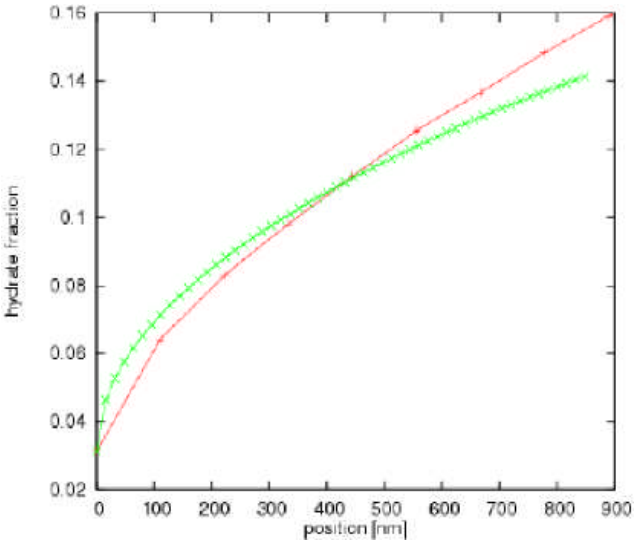

Fig. 8 Comparisons between phase field theory and (green) and cellular automata (red) for CO_2 hydrate growing from saturated aqueous solution of CO_2 at 150 bar and 1 °C.

IV Discussion

There is a lack of experimental information to compare the simulations to. Tohidi et.al.[34] have indicated an average growth rate of 55 micrometer per second. Our results are not directly comparable since their experimental conditions are different and our simulations are shorter in time. If we ex-tend our results under the assumption that the rate is con-trolled by mass diffusion the agreement with the experimental results are in fair agreement when considering the differences in thermodynamic driving forces.

With the Japanese research program MH21, aiming at exploitation of hydrate reservoirs from 2016 several scientific environments in Japan and elsewhere are conducting reservoir simulations of possible exploitation scenarios. One of the most limiting factors of these simulations are the lack of reliable kinetic models for the fluid/hydrate phase transitions. Exploitation of hydrate reservoirs using CO_2 represents a win-win situation since there is a natural thermodynamic driving force in the higher thermodynamic stability of the CO_2 hydrate relative to the methane hydrate and the final state represents a long term storage solution for CO_2. The free energy functional for this system is given by equation (10) and the corresponding thermodynamics is also discussed. More details on the thermodynamic models can be found in Svandal et.al.[39]. Work is yet in progress on the simulation of the reformation kinetics and a highly preliminary result is presented in fig. 9 below.

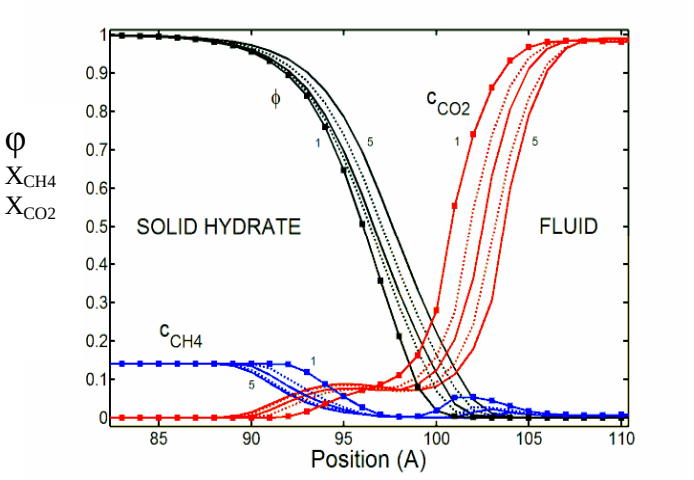

Fig. 9. Time evolution of the phase field (black), the CO_2 concentration (red), and the CH_4 concentration (blue). The five curves correspond to times t = 0.1, 0.5, 1, 1.5 and 2.7 ns.

V Conclusions

Phase field theory simulations have been applied to model the growth of CH_4 and CO_2 hydrates from respective aqueous solutions of these hydrate formers.

Presently there are no experimental data available for direct comparisons to the predictions presented here and the main purpose of this pa-per has been to demonstrate the approach and the corresponding parameterization. As expected relative to the differences in solubility of the two components in water the kinetic rates of CO_2 hydrate growth is larger than that of CH_4 hydrate. The rate of circular growth is larger than the corresponding growth on a planar interface but in both cases the kinetics is dominated by the mass transport of solutes towards the growing front. We have also investigated the effects of anisotropy. The growth of dendrites is faster than for isotropic growth and are approaching a constant rate. The phase field theory simulations also shows the expected non-uniform growth patterns at the interface between fluid CO_2 and saturated aqueous solution of CO_2.

Work is also in progress towards simulations of hydrate growth in porous media and a first simple approach for solid material has been investigated in this work. As expected due to free energy gradient hydrate initiation and growth is favored in inclines. The agreement between phase field theory and cellular automata is fairly good at small time steps but the slopes indicate significant deviations at large times.

Phase field theory simulations have been applied to model the growth of CH_4 and CO_2 hydrates from respective aqueous solutions of these hydrate formers. Presently there are no experimental data available for direct comparisons to the predictions presented here and the main purpose of this paper has been to demonstrate the approach and the corresponding parameterization. As expected relative to the differences in solubility of the two components in water the kinetic rates of CO_2 hydrate growth is larger than that of CH_4 hydrate. The rate of circular growth is larger than the corresponding growth on a planar interface but in both cases the kinetics is dominated by the mass transport of solutes towards the growing front. We have also investigated the effects of anisotropy. The growth of dendrites is faster than for isotropic growth and are approaching a constant rate.

Acknowledgments

This work has been supported by the Norwegian Research Council under project Nos. 153213/432 and 151400/210. Financial support from Hydro also acknowledged. Phase Field solutions are based on the coding due to Laszlo Granasy which also provided figure 9.

References

1. L. Milich, Global Environmental Change – Human and Policy Dimensions **9**, 179 (1999).
2. Bünz, S., Mienert, J., Berndt, C., 2003. Geological controls on the Storegga gas-hydrate system of the mid-Norwegian continental margin. Earth and Planetary Science Letters, 209 (3-4), 291-307Storegga
3. Zweigel, P., Hamborg, M., Arts, R., Lothe, A., Sylta, Ø., and Tømmer°as, A., 2000. Results and experiences from the first industrialscale underground CO_2 sequestration case (Slepiner Field, North Sea), American Association of Petroleum Geologists, Annual Meeting, June 2001, Denver, abstract volume (CD) 6p.
4. a) B. Kvamme, A. Graue, E. Aspenes, T. Kuznetsova, L. Gránásy, G. Tóth, and T. Pusztai, Phys. Chem. Chem. Phys. **6**, 2327 (2004), b) Granasy, L., Pusztai, T., Tegze, G., Kuznetsova, T., Kvamme, B. in *Recent review on gas hydrate research: Advances in the Study of Gas Hydrates*, eds. C. E. Taylor and J. T. Kwan (Springer, Berlin, 2004).
5. Gránásy, L., Pusztai, T., Jurek, Z., Conti. M., Kvamme, B., Phase field theory of nucleation in the hard sphere liquid. *J.Chem.Phys*., 2003, 119, 10376 – 10382
6. Gránásy, L., Pusztai, T., Börzsönyi, T., Warren, J. A., Kvamme, B., James, P. F., Nucleation and polycrystalline solidification in binary phase field theory. Physics and Chemistry of Glasses, 2004, 45, 107 – 115
7. L. Gránásy, T. Börzsönyi, and T. Pusztai, J. Cryst. Growth **237-239**, 1813 (2002)
8. L. Gránásy, T. Pusztai, J. A. Warren, J. F. Douglas, T. Börzsönyi, and V. Ferreiro, Nature Mater. **2**, 92 (2003)
9. L. Gránásy, T. Pusztai, T. Börzsönyi, J. A. Warren, and J. F. Douglas, Nature Mater. **3**, 645 (2004)
10. L. Gránásy, T. Pusztai, and J. A. Warren, J. Phys.: Cond. Matter **16**, R1205 (2004)
11. T. Pusztai , G. Bortel, L. Gránásy: Europhys. Lett. **71**, 131 (2005)
12. J. A. Warren and W. J. Boettinger, Acta Matell. Mater. **43**, 689 (1995).
13. S. L. Wang, R. F. Sekerka, A. A. Wheeler, B. T. Murray, S. R. Coriell, R. J. Braun, and G. B. McFadden, Physica D **69**, 189 (1993).
14. Buanes, T., Kvamme B.: *"Computer simulation of CO_2 hydrate growth Two approaches for modelling hydrate growth".* J. Cryst. Growth. in press, 2005
15. Oxtoby, D.W., "Density functional methods in the statistical mechanics of materials", Annual Review of Materials Research, 2002, 32, 39-52
16. Rehder G., Kirby S.H., Durham W.B., Stern L.A., Peltzer E.T., Pinkston J., Brewer P.G.: Dissolution rates of pure methane hydrate and carbon-dioxide hydrate in undersaturated seawater at 1000-m depth. *Geochemica et Cosmochimica Acta,* 68, 285-292, 2004.

17. Radhakrishnan R., Demurov A., Herzog H., Trout B.L.: A consistent and verifiable macroscopic model for the dissolution of liquid CO_2 in water under hydrate forming conditions, *Energy Conversion and Management*, 44, 771-780, 2003.
18. Davidchack, R. L.; Laird, B. B. J. Chem. Phys., 1998, 108, 9452.
19. Hoyt, J.J., Asta, M., Karma, A., J. Chem. Phys. **86**, 5530 (2002)
20. Hoyt, J.J., Karma, A., Phys. Rev. B **65**, 214106 (2002)
21. Asta, M., Hoyt, J.J., Karma, A., Phys. Rev. B **66**, 100101 (2002)
22. Morris, J.R., Phys. Rev. B. **66**, 144104 (2002)
23. Cahn, J. W., Hilliard, J. E., J. Chem. Phys. **28**, 258 (1958).
24. Buanes, T., Kvamme, B., Svandal, A. *Computer simulation of CO_2 hydrate growth*. Journal of Crystal Growth. In Press.
25. Buanes, T., Kvamme, B., 2005, *Computer simulation of CO_2 hydrate growth* Presented at the 16th American Conference on Crystal Growth and Epitaxy (ACCGE 16) July 10-15,2005
26. Span R., Wagner W. J. Phys. Chem. Ref. Data, 25, 1509-1596, 1996.
27. Diamond L.W., Akinfiev N.N.: Solubility of CO_2 in water from -1.5 to 100 °C and from 0.1 to 100 MPa: evaluation of literature data and thermodynamic modelling. *Fluid Phase Equilibr.*, 208, 265-290, 2003.
28. Soave, G. Chem. Eng. Sci., 27, 1197, 1972.
29. Lekvam K., Bishnoi P.R. Fluid Phase Equilibria, 131, 297-309, 1997
30. R. Anderson, M. Llamedo, B. Tohidi, and R. W. Burgass, J. Phys. Chem. B **107**, 3507 (2003)
31. Hardy, S. C. Philos. Mag., 1977, 35, 471
32. Berendsen, H.C.J, Gridera, .J.R., Strastmaa, T.P. J. Phys. Chem. 91, p. 6269-6271 (1987)
33. Harris, J.G., Yung, K.H. J., Phys. Chem. 99, pp. 12021 – 12024 (1995)
34. Gránàsy L., Börzsönyi T., Pusztai T. Phys. Rev. Lett., 88, 206105, 2002.
35. Warren J.A., Boettinger W.J. Acta metall. mater. 43, 689-703, 1995.
36. Kvamme, B., Kuznetsova, T., Uppstad., D., 2005, *Modeling excess surface energy in dry and wetted calcite systems.* Submitted to Journal of Material Science, December 2005
37. Kvamme, B., Kuznetsova, T., 2005, *Investigation into stability and interfacial properties of CO_2 hydrate - aqeuous fluid system.* Submitted to Journal of Computational Methods in Sciences and Engineering December 2005
38. Tohidi, B., Anderson, R., Clennell, .., Burgass, R.W., Biderkap, A.B., *Geology;* 29, p. 867–870, 2001
39. Svandal, A., Kuznetsova, T., Kvamme, B., " Thermodynamic properties and phase transtions in the $H_2O/CO_2/CH_4$ system", Physical Chemistry Chemical Physics, 2006, in press